Polymer Journal (2024) 56:541–551
https://doi.org/10.1038/s41428-023-00879-1

ORIGINAL ARTICLE

Improving the electro-optical properties of cholesteric liquid crystal devices via cellulose nanoparticle dopants

Chung-Yu Kuo[1] · A. V. Emelyanenko[2] · Sheng-Chi Hung[1] · Wei-Chuan Chen[1] · Chun-Yen Liu[1]

Received: 13 October 2023 / Revised: 23 November 2023 / Accepted: 10 December 2023 / Published online: 12 January 2024

Abstract

In the presence of a strong electric field, helices in a cholesteric liquid crystal (CLC) phase might be unwound, leaving liquid crystal (LC) molecules parallel to the electric field, thereby realizing transparency. Previously, we developed a novel particle-doped CLC cell without alignment layers that exhibited liquid crystal display (LCD) capabilities via electro-optical properties. This ability represents a novel advancement in LCD fabrication, resulting in enhanced electro-optical characteristics. To explore the impact of chirality on LCDs, we synthesized and radially constructed cellulose particles. These were then employed as chiral dopants in the production of LCD cells. The fabricated chiral nanoparticle (CNP)-doped PC05 CLC cell showed a high transparency of 97.4% and a fast response time of 7.6 ms. For the prepared radially constructed PDAT-doped PD2T PSCLC cell, a high transmittance of 93.6% and a fast response time of 13 ms were achieved. Fabrication of LCD cells without an alignment layer on substrates was achieved by indicate adding polymeric chiral nanoparticles into CLC mixtures. Adding 2 wt% chiral CNPs promoted the transmittance of the CLCs from 3.4 to 97%. This novel chiral dopant technique enables the use of a new easy method for the fabrication of LCDs.

Introduction

The cholesteric phase is also known as the chiral nematic phase because it is the chiral version of the nematic phase. Achiral liquid crystals can form a chiral nematic phase upon addition of a small amount of chiral dopant, yielding a substance with high helical twisting power. This process is proposed to be accomplished by chiral additives that produce a chiral environment for all the other achiral molecules, resulting in a helical macrostructure [1–5].

Cholesteric liquid crystal (CLC) cell textures are particularly sensitive to electric fields [6–11]. If the applied electric field between two slides is strong enough, then the helices in the CLC phase can unwind, and the corresponding liquid crystal (LC) molecules would parallel the electric field in the homeotropic texture [12–15], thus exhibiting transparency. Theoretically, a light shutter or smart CLC window can be created by switching between the focal conic and homeotropic textures [16–21].

Much research has explored the concept of additives in liquid crystal systems to improve the physical properties, such as the electric, optical, and magnetic properties, of liquid crystal devices (LCDs). Carbon nanotubes (CNTs) [22–24], nanoparticles (NPs) [25–28], quantum dots (QDs) [29, 30] and graphene oxide flakes [31–33] are often doped into LC or polymer-stabilized liquid crystal (PSLC) systems. NPs are the most popular dopant in these applications due to their effects on electro-optical performance and LC alignment. For QDs with different concentration effects on polymer-stabilized cholesteric liquid crystal (PSCLC) devices, the addition of CdSeS/ZnS QDs reduces the threshold voltage due to the correspondingly reduced anchoring strength, while the sulfur-based shell in the QD structure also reduces the response time of the PSCLC device [34, 35]. Plasmon resonance on the surface of silver and gold NPs causes an increase in the dielectric response, and the optical characteristics can be modified based on size, shape, distribution, and other parameters [36–41].

Supplementary information The online version contains supplementary material available at https://doi.org/10.1038/s41428-023-00879-1.

✉ Chun-Yen Liu
cyliu@gs.ncku.edu.tw

[1] Department of Materials Science and Engineering, National Cheng Kung University, Tainan 701401, Taiwan

[2] Faculty of Physics, Lomonosov Moscow State University, Moscow 119991, Russia

Surface treatment easily functionalizes these metal NPs. As a result, several studies have investigated the interaction between metal NPs and the LC host [42–44]. To the best of our knowledge, no study has reported the use of polymeric beads as additives for the fabrication of LCDs.

In our previous paper, we developed a novel polymer bead-dispersed liquid crystal device (PBLCD) using radially constructed polydopamine (PDA) particles as additives for the fabrication of liquid crystal devices [45]. Improving upon traditional and complicated processes, a more straightforward method for the fabrication of LCDs was achieved. Considering the chiral twisting power of liquid crystals, to study the chiral effect of polymer dopants on the improvement of the electro-optical properties of PBLCD, in this study, both chiral hydroxypropyl cellulose nanoparticles (CNCs) and radially constructed CNCs were used. The performance of these compounds were compared with that of achiral radially constructed PDA nanoparticles. Several significant chiral effects on the improvement of electro-optical properties of the fabricated LCDs were observed.

Experimental section

Materials

2-Methyl-1,4-phenylene bis(4-(3-(acryloyloxy)propoxy) benzoate) (RM257), 4'-[(S)-2-methylbutyl]biphenyl-4-carbonitrile (CB 15) and Irgacure-184 were purchased from Fusol Material Corp. (Tainan, Taiwan), Luminescence Technology Corp. (Taipei, Taiwan) and Alfa Aesar (Massachusetts, USA), respectively. 3-Hydroxytyramine hydrochloride (dopamine hydrochloride) and dimethyloctadecyl-3-(trimethoxysilyl) propyl ammonium chloride (60% in methanol, DMOAP) were obtained from Acros Organics (Belgium, Germany). Indium tin oxide (ITO) glass and spacers were purchased from Uni-Onward Corp. (New Taipei, Taiwan) and Shinkong Synthetic Fibers Corp. (Taipei, Taiwan), respectively. Desulfated cellulose nanocrystals (DS-CNCs) were purchased from Cellulose Lab (Toronto, Canada). All the commercial chemicals used in this research were ACS grade or higher and were used without further purification.

Instruments

Phase transition temperature and optical texture variations were further studied using a polarized light microscope (POM, Nikon ECLIPSE C*i* POL, Tokyo, Japan) equipped with a hot stage (LINKAM T96-S, London, England), and the experimental temperature scanning rate was determined to be 10 K min^{-1}. The phase transitions of all the liquid crystal mixtures were investigated with a differential scanning calorimeter (DSC, PerkinElmer DSC 7, Massachusetts, United States) at a heating/cooling rate of 10 K min^{-1}. Thermal stability data were recorded under a nitrogen atmosphere at a heating rate of 10 K min^{-1} with a thermogravimetric analyzer (TGA, PerkinElmer TGA 7, Massachusetts, United States). As shown in Fig. S1, the electro-optical properties of the fabricated cells were estimated using a configuration consisting an arbitrary/function generator (Tektronix AFG3021B, Oregon, United States), a digital storage oscilloscope (Tektronix TDS 2014b, United States), a high-voltage amplifier (PINTEK HA-805, New Taipei, Taiwan), a photodetector (Electro-Optics Technology ET-2000 Silicon Pin Detector, Miami, United States) and a helium–neon laser (Meredith Instruments, Arizona, United States). The physical properties of the PDA and cellulose nanoparticles were analyzed using a dynamic light scattering spectrophotometer (DLS, Otsuka ELSZ-1000ZS, Taipei, Taiwan), Fourier transform infrared spectroscopy (FTIR, Jasco FTIR-4600, Tokyo, Japan) and scanning electron microscopy (SEM, JOEL, HR-FESEM 6700F, Tokyo, Japan).

Synthesis of polymeric particles

Synthesis of PDA beads

As we described previously, dopamine hydrochloride (0.2 g) was dissolved in a mixture of 50 ml of deionized (DI) water and 20 ml of ethanol [45]. A diluted sodium hydroxide aqueous solution was used to adjust the pH of the dopamine solution to 10. Upon addition of the sodium hydroxide, the color of the reaction mixture became orange and then black. Figure S2 shows the synthetic process of polydopamine nanoparticles. After mixing the reagents, the mixture was stirred at 300 rpm at 30 °C for 24 h. After the reaction, a dark black reaction mixture was obtained. The synthesized PDA particles in the product solution were centrifuged at 6000 rpm for 10 min. The synthesized crude product was washed three times with DI water. The PDA particles were frozen in a small amount of water for 2 days and then ground to a fine powder.

Modification of PDA particles with DMOAP

The prepared PDA powder was dispersed in a 1.5 wt% DMOAP aqueous solution. This mixture was treated under ultrasonic oscillation for 25 min to form a layer of DMOAP molecules on the surface of the PDA particles. The DMOAP-modified PDA particles were denoted as PDAT particles. The synthesized crude solution was centrifuged at 5000 rpm for 15 min, followed by washing with DI water three times to remove unreacted DMOAP. The synthesized PDAT particles were frozen in a small amount of water for

2 days and then ground to a fine powder. This modification process is shown in Fig. S3.

Modification of cellulose nanoparticles with DMOAP

The DMOAP solution (1.25 g, 60%) was mixed with DI water (50 ml) to prepare a 1.5 wt% DMOAP aqueous solution, after which the commercially available cellulose nanoparticles (CNPs) were dispersed in the solution. The cellulose nanoparticles were treated in a DMOAP aqueous solution under ultrasonic oscillation for 20 min to form a layer of DMOAP molecules on the surface of the cellulose nanoparticles. The DMOAP-modified cellulose nanoparticles used in this study were named CNPT particles. The crude solution was centrifuged at 10,000 rpm for 10 min and then washed three times with DI water to remove unreacted excess DMOAP in the solution. The synthesized CNPT particles were freeze-dried for 2 days and subsequently ground to a fine powder. The process of modifying the cellulose nanoparticles is shown in Fig. S4.

Preparation of cholesteric liquid crystal cells

Cleaning of ITO-coated glass substrates

The ITO-coated glass substrates were cut into 25 mm × 25 mm squares with a thickness of 0.7 mm. These substrates were washed with neutral detergent for 15 min in an ultrasonic cleaner and then washed with DI water two times, each time for 15 min. For the last cleaning step, acetone was applied to wash the substrates in an ultrasonic cleaner for 30 min. The cleaned ITO-coated glass substrates were dried in an oven for at least 2 h and were thus ready for use in the following experiments.

Fabrication of sandwiched ITO cells

As illustrated in Fig. S5, one ITO glass slide overlapped face-to-face with the other slide. The overlapping area was determined as 21 mm × 17 mm. Then, two spacers with a thickness of 25 μm (18 mm × 2 mm in size) were placed between two indium tin oxide (ITO) glasses to form a gap for subsequent liquid crystal material injection. The edges of the assembled ITO cells were enclosed with epoxy glue and dried for 2 days to prevent possible leakage. The prepared ITO cells were used for further studies.

Preparation of the CLC mixture

A cholesteric liquid crystal (CLC) mixture was prepared by homogenously mixing both commercially available nematic liquid crystal (NLC) MJ05581 and the 5 wt% chiral dopant CB15. The physical properties of MJ05581 are shown in Table S1.

Polymeric particle-doped CLC mixtures

The prepared PDA, PDAT, CNP and CNPT particles were dispersed in chloroform to form dispersions. After ultrasonic oscillation for 10 min, the dispersion was immediately dropped into the prepared CLC mixture. The concentration of particles dispersed in the LC mixtures was predetermined to be in the range of 0.05 to 0.2 wt%. In accordance with the concentration, samples doped with 0.05, 0.1 and 0.2 wt% PDA nanoparticles are denoted D05, D1 and D2, respectively. The "T" denotes the regular and CNP nanoparticles modified with DMOAP. A few drops of chloroform were used to prepare homogeneous mixtures with stirring at 300 rpm for 2 days. After removing the solvent, the mixture was ultrasonically oscillated for 10 min to prevent particle aggregation.

Fabrication of particle-doped CLC cells

The particle-doped CLC mixture was heated to 75 °C to form an isotropic phase and then injected into the prepared sandwiched ITO cells by capillary phenomena. The cells were held at 75 °C for 10 min for homogenization. These cells were then removed from the hot plate and gradually cooled to room temperature. The fabricated particle-doped CLC cells were maintained for further study.

Fabrication of polymer-stabilized particle-doped CLC cells

To compare the electro-optical properties of the fabricated particle-doped CLCs, polymer-stabilized cholesteric liquid crystal (PSCLC) cells were prepared in this study. To fabricate the PSCLC, 2 wt% RM257 with 0.4 wt% photoinitiator was added to the previously prepared CLC mixture with an external electric voltage (40 V) across the cell and then exposed to UV irradiation (365 nm, 5 mW/cm^2) for 3 min. The fabricated PSCLC cells exhibited a scattering state without an applied electric field, whereas a transparent state was observed with an applied electric field (>V_{th}).

The chemical structures used for the PDA particle-doped and CNP-doped CLC and PSCLC devices are shown in Scheme 1.

Measurement of electro-optical properties

The prepared CLC and PSCLC cells with PDA, PDAT, CNP and CNPT particles were prepared under DC voltage, which was generated by the combination of a high-voltage amplifier, function generator and digital storage oscilloscope. The transmittances of the CLC and PSCLC cells were measured by a photodetector, which can convert the light intensity to an electrical signal. The transmittance was calibrated by an empty sandwiched ITO cell. As shown in

Scheme 1 Chemicals used for the CLC and PSCLC mixtures

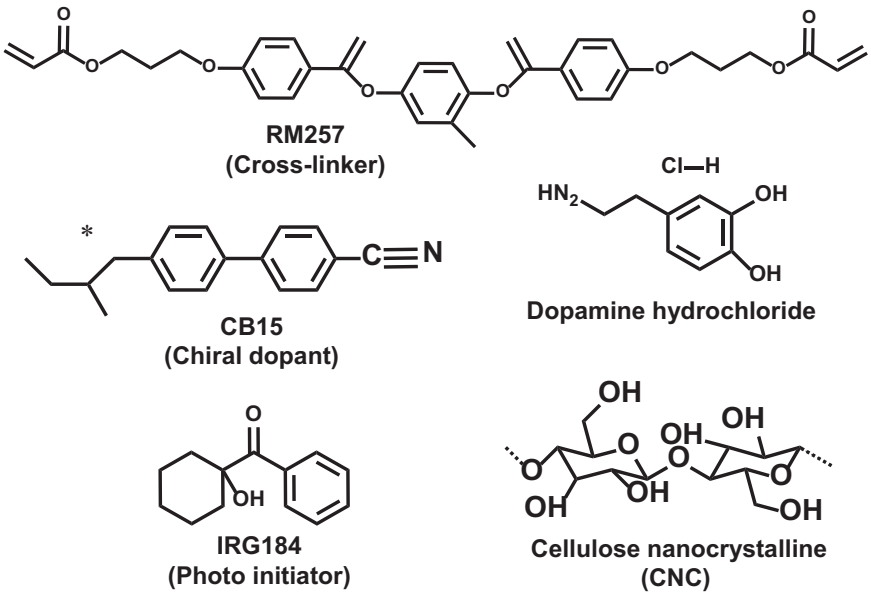

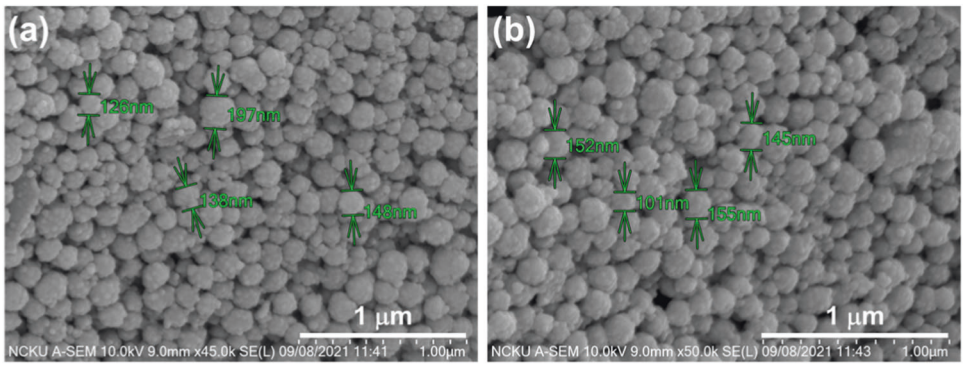

(c)

Particles	Mean Size*	Minimum	Maximum	Standard Deviation
PDA	140	101	155	21.8
PDAT	160	134	198	27.8

*In nanometer

Fig. 1 SEM images of (**a**) PDA and (**b**) PDAT particles and (**c**) the distribution of PDA and PDAT particle sizes

Fig. S1, the electro-optical properties of the fabricated LCDs were measured with a laser system with a helium–neon laser light source (632.8 nm).

Results and discussion

Characterization of polymer particles

SEM image of PDA particles

Polydopamine (PDA) particles were prepared and modified with a DMOAP aqueous solution to obtain PDAT particles. Both PDA and PDAT particles were ground into black fine powders and analyzed via SEM to evaluate the particle sizes of the synthesized particles. Figure 1a, b shows sphere-like particles with a rough surface. The mean sizes of the synthesized PDA and PDAT particles were calculated to be 140 nm and 160 nm, respectively. Figure 1c shows that the PDAT particles were slightly larger than the PDA particles were, revealing a wider particle size distribution after the DMOAP coating process.

Hydrophilicity of PDA particles

Figure S6a shows the molecular structure of DMOAP, which is commonly utilized for perpendicular alignment on glass surfaces for LC devices. Due to the long carbon chain of the DMOAP molecule, DMOAP can force the LC molecules to align in the direction perpendicular to the

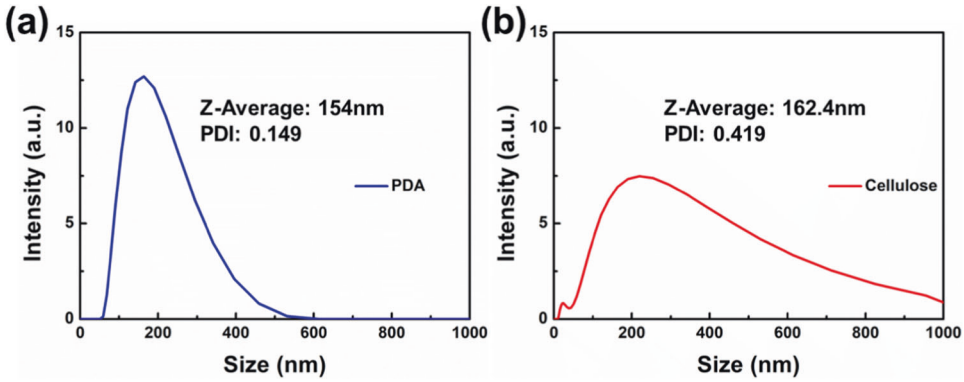

Fig. 2 Dynamic light scattering (DLS) analysis of (**a**) PDA and (**b**) cellulose nanoparticles (CNPs)

particle surface. As illustrated in Fig. S6b, PDAT particles with DMOAP molecule surface coatings were predicted to yield a radial alignment on the particle surface to interact with LC molecules. In CLC mixtures, PDAT particles demonstrated greater size dispersion, and a strong interaction between particles and LC molecules was expected. Figure S6c shows the difference in hydrophilicity between PDA and PDAT particles in DI water. PDA particles possess a hydrophilic surface because the particles are well dispersed in water, whereas the PDAT particles aggregate and are suspended in water. This outcome is attributed to the change in particle surface properties from hydrophilic to hydrophobic following surface modification with DMOAP. To further confirm the presence of DMOAP on the surface of the PDAT particles, FTIR was used to measure the DMOAP layer via spectral subtraction between PDA and PDAT, as shown in Fig. S6d.

Dynamic light scattering (DLS) analysis of particles

The synthesized PDA nanoparticles and commercially available desulfated cellulose particles (CNPs) were analyzed using a DLS spectrophotometer. Before the measurement, the nanoparticles were dropped into DI water and placed in a cuvette. The estimated dispersity and average size of the PDA and cellulose particles are shown in Fig. 2. The average size of the PDA particles was ~154 nm, whereas the average size of the cellulose nanoparticles (CNPs) was ~162.4 nm. Similar sizes of both PDA and cellulose nanoparticles are beneficial for comparing the structure and material effect of dopants dispersed in liquid crystals.

Characterization of cholesteric liquid crystal cells

POM textures of CLC cells

To further study the POM textures, a sample cell with a pair of antiparallel alignment layer substrates was prepared. Various cholesteric textures were observed under a polarized optical microscope (POM). Figure S7 shows the POM textures of the CLC mixture heated at a rate of 5 °C/min in the liquid crystal cell. Figure S8 shows the (1) DSC curve of the CLC mixtures and (2) the calculated clearing temperature. Figure S8 of the Supporting Information shows that the introduction of dopants confirmed the alterations in the clearing temperature of the liquid crystal mixtures. These findings indicate a substantial interaction between the introduced particle dopants and the liquid crystals. Based on the results, the fabricated sample cell exhibited an isotropic phase at 80 °C, as shown in Fig. 3a, and the liquid crystals were arranged randomly. During this time, the polarized incident light is unable to pass through the analyzer, resulting in a dark image. When the sample cell was cooled to ambient temperature, Bragg reflection occurred when the liquid crystals were aligned in a planar state, and the incident light that passed through the LCs was rotated, resulting in the appearance of a planar texture, as illustrated in Fig. 3b. For comparison, an LC cell with substrates without any alignment layer was prepared. The randomly dispersed CLC helices in the cell created a focal conic texture without surface alignment layers, as shown in Fig. 3c. When an electric voltage was applied to the cell, the liquid crystals aligned parallel to the electric field, which disabled the rotation of the polarized incident light and resulted in a black image, as shown in Fig. 3d. The homogeneous dark image indicates that the LC molecules aligned in a homeotropic alignment parallel to the electric field. The inset images in Fig. 3 illustrate this LC molecule alignment.

Particle-doped CLC cells

PDA and PDAT particles were dispersed in CLC mixtures at concentrations ranging from 0.05 to 0.2 wt%. The compositions of the CLC mixtures with various amounts of dopants are listed in Table 1. Both the PDA and PDAT particle-doped mixtures reached a uniform distribution after removal of the solvent. The results indicate that the PDA and PDAT particles can be dispersed in high-viscosity LC mixtures. The prepared PDA-doped CLC mixtures and PDAT-doped CLC mixtures were used for further studies.

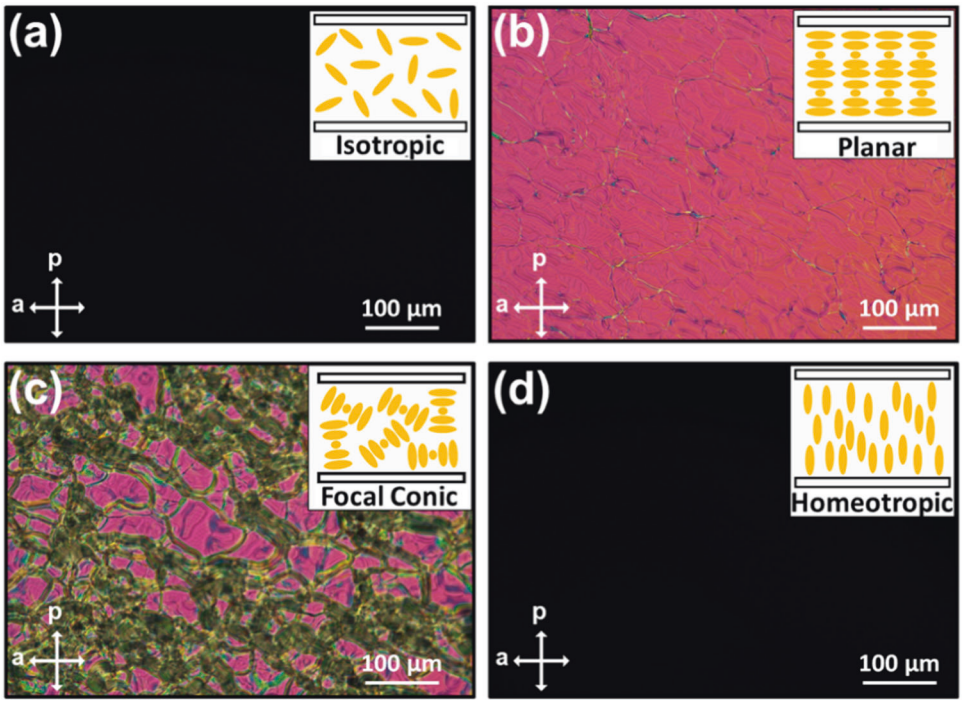

Fig. 3 POM textures of the CLC mixture under the (**a**) isotropic state, (**b**) planar state, (**c**) focal conic state, and (**d**) homeotropic state under 40 V switching

Table 1 Estimated response time of PSCLC cells[a]

Code	T_{ON}[b]	T_{OFF}[c]	Average
CLC	36.4	12.0	24.2
PSCLC	150.0	12.4	81.2
PD2T	16.8	9.2	13.0
PC2T	49.0	11.0	30.0
PD05	15.1	8.5	11.8
PC05	10.3	7.6	9.0

[a]Response time in ms

[b]Turned on response

[c]Turned off response

As shown in Table S2, cellulose nanoparticles (CNPs) and radially constructed cellulose particles (CNPTs) were also dispersed in CLC mixtures at concentrations ranging from 0.05 to 0.2 wt%. The prepared CNP-doped CLC mixtures and CNPT-doped CLC mixtures were used for further investigations.

Electro-optical properties of particle-doped CLC cells

The switching performances of PDA particle-doped CLC cells were then measured with a discontinuous increasing voltage. Figure S9 shows the dependence of the transmittance of (1) CLC, (2) 0.1 wt% PDA particles, and (3) 0.1 and (4) 0.2 wt% CNP particle-doped CLC cells on the electric field discontinuously increasing from 0 V to 40 V. Based on the results of all the prepared sample cells, the calculated sample cell transmittances are summarized in Fig. 4a, b. As shown in Fig. 4b, 96.9% transmittance was achieved via CNP particle doping. To investigate the radial construction effect on CLC cells, DMOAP surfactant-treated PDAT and CNPT particle-doped sample cells were tested. The results are summarized in Fig. 5. As shown in Fig. 5a, b, the observed maximum transmittance decreased compared with that shown in Fig. 4. These results are ascribed to the aggregation of surface-treated particles. Figure S6a shows the molecular structure of DMOAP. Surface-modified particles may aggregate due to interactions between radially constructed long hydrophobic carbon chains, leading to a decrease in transmittance.

Particle-doped PSCLC cells

To further study the effect of radially constructed dopants on PSCLC cells, a series of PSCLC cells were prepared. Table S3 shows the compositions of these PSCLC sample cells. A PSCLC mixture containing 2 wt% RM257 and 0.4 wt% photoinitiator was used. Figure S10 shows the (1) DSC curve of the PSCLC mixtures and (2) the calculated clearing temperature. Like for the CLC mixtures, the clearing temperatures are close to 70 °C.

Electro-optical properties of particle-doped PSCLC cells

To study the effect of particle dopants on PSCLC cells, PSCLC cells without particle dopants and PSCLC cells with various particles and surface-treated particle-doped sample

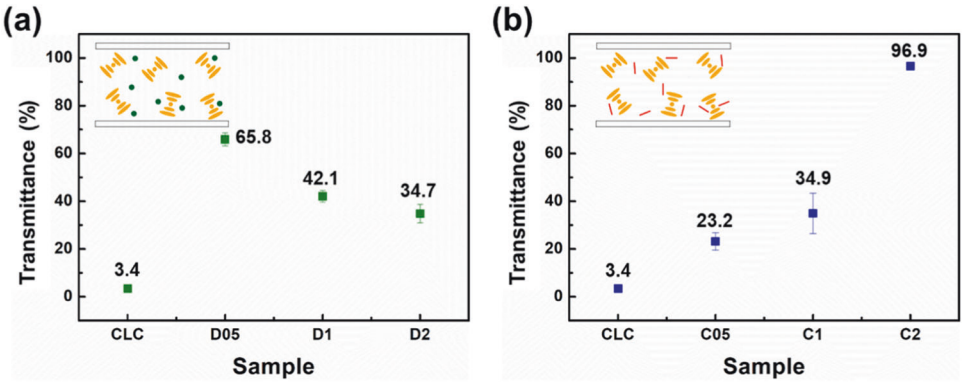

Fig. 4 Calculated transmittance of the (**a**) PDA and (**b**) CNP particle-doped CLC sample cells

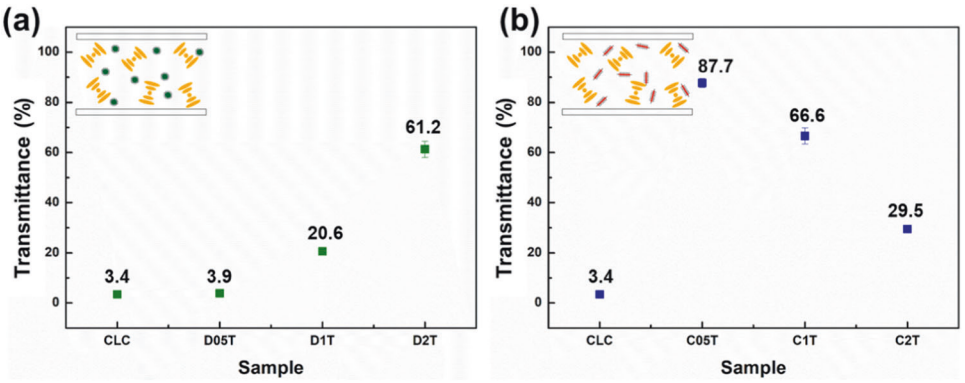

Fig. 5 Calculated transmittance of the (**a**) PDAT and (**b**) CNPT particle-doped CLC sample cells

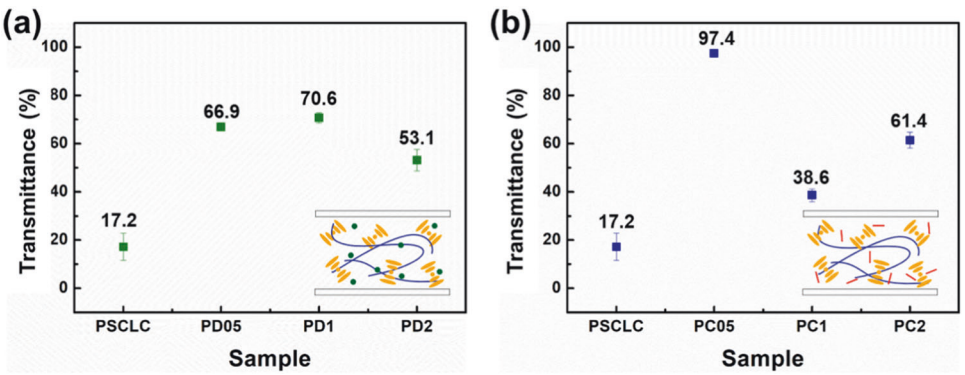

Fig. 6 Calculated transmittance of the (**a**) PDA and (**b**) PCNP particle-doped PSCLC sample cells

cells were fabricated. As shown in Fig. 6, without the particle dopant, the PSCLC cell shows only 17.2% calculated transmittance. Adding PDA and CNP dopant particles increased the transmittance to 70.6% and 97.4%, respectively. Notably, as shown in Fig. 4b, the chiral CNP particles had a significant chiral effect on the PSCLC cells, leading to a high transmittance of 97.4%.

Figure 7 shows the calculated transmittances of the (1) PDAT and (2) PCNPT particle-doped PSCLC sample cells. Unlike in CLC cells, polymer-stabilized CLC cells inhibited the aggregation of surface-treated particles, leading to an increase in the maximum transmittance to 93.6% for PD2T cells. However, as shown in Fig. 7b, surface radial treatment decreased the chiral effect, leading to a decrease in the maximum transmittance to 84.9%. In addition, without particle doping, the prepared CLC cells and PSCLC cells exhibited a low transmittance of 17.2%.

Response times of the PSCLCs

The response times of the prepared PSCLC sample cells were measured to estimate the response times of both PDAT and PCNPT particle-doped PSCLC cells. Figure 8 shows the electrical response of PSCLC cells to various dopants, $PD2T_{ON}$, $PD2T_{OFF}$, $PC2T_{ON}$ and $PC2T_{OFF,}$ at an operating voltage of 40 V. Figure 8a, c and b, d indicates cell transmittance variations during the "ON" state and "OFF" state, respectively.

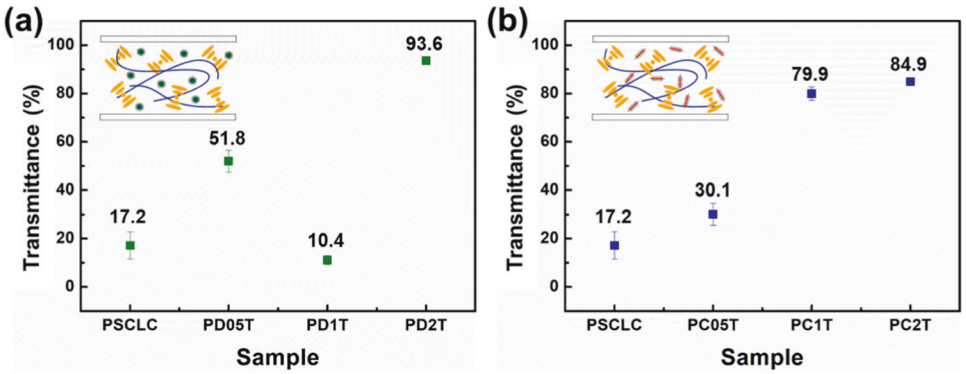

Fig. 7 Calculated transmittance of the (**a**) PDAT and (**b**) PCNPT particle-doped PSCLC sample cells

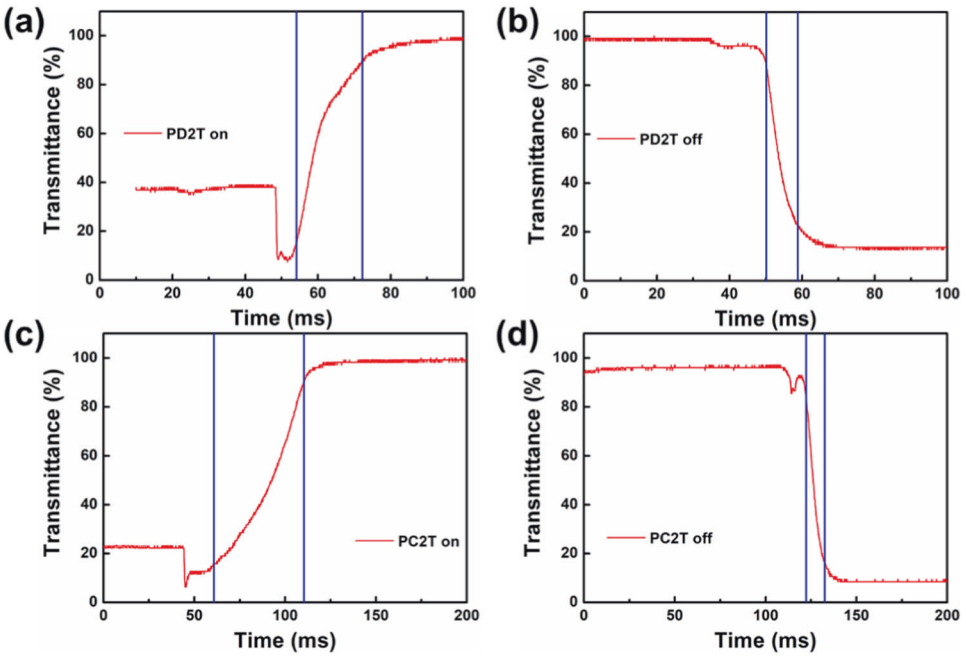

Fig. 8 Electrical response of PSCLC cells with various dopants (**a**) $PD2T_{ON}$, (**b**) $PD2T_{OFF}$, (**c**) $PC2T_{ON}$ and (**d**) $PC2T_{OFF}$, via an operating voltage of 40 V

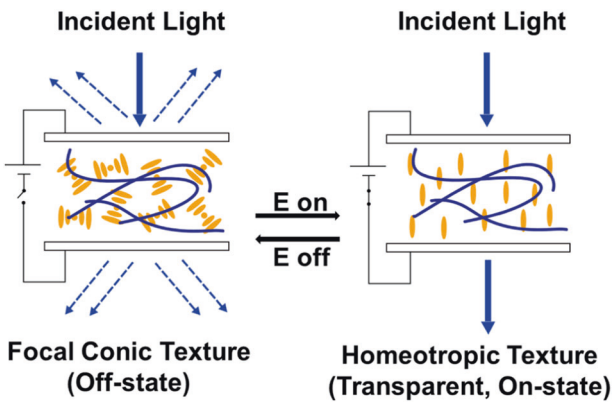

Fig. 9 Schematic illustration of CNP particle-doped PSCLC cells

Table 1 shows the estimated response times of the fabricated CLC and PSCLC sample cells. Notably, without particle dopants, the PSCLC cell exhibited a 150 ms response time when the cell was turned "ON". Compared with that of particle-doped sample cells, the response time is quite slow. The added particle dopants may reduce the resistance of the polymer matrices, resulting in a lubricating effect on the LC molecules and a rapid response. For humans, vision resistance is ~62 ms, and the results summarized in Table 1 indicate that the prepared PD2T and PC2T cells are suitable for the television LCD designation. PC05 showed a faster response than PC2T. Figure 9 shows a schematic illustration of the CNP-doped PSCLC cell. A higher concentration of chiral dopant increases the twisting power of the CLC mixture, increasing the driving force from being focal-conic being to homeotropic, thereby increasing the response time. Furthermore, surface-treated radial constructions may disturb the movement of CNP particles in polymer matrices.

Performance as a light shutter

Images of the PC05 cell used as a light shutter under 40 V switching are shown in Fig. 10. When the sample cell was

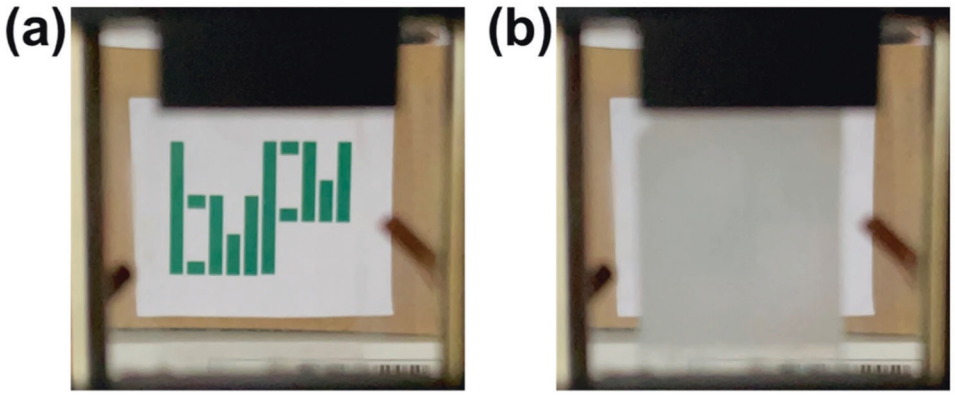

Fig. 10 Real images of PC05 cells switching to the (**a**) transparent "ON" state and (**b**) opaque "OFF" state; a colorful image was taken behind the LC cell

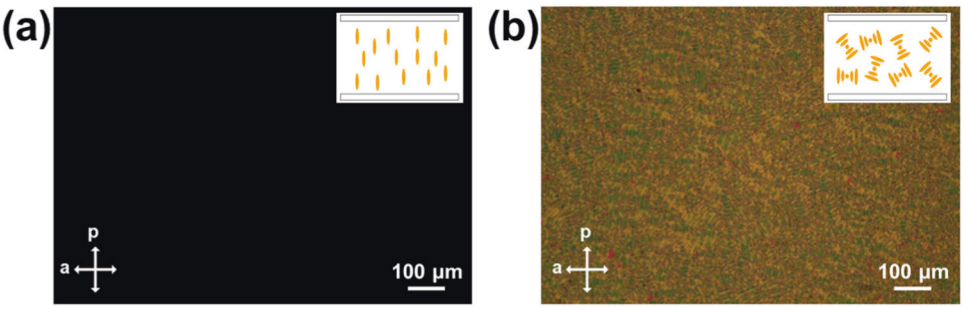

Fig. 11 POM textures of PC05 cells in the (**a**) "ON" state and (**b**) "OFF" state

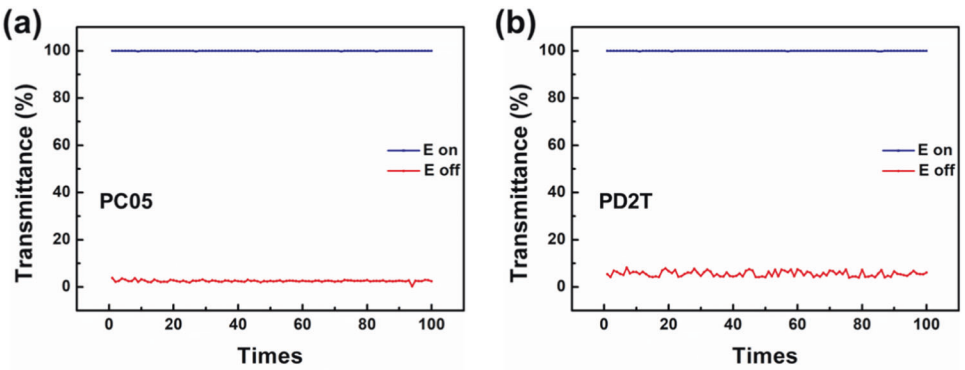

Fig. 12 Reliability of the fabricated (**a**) PC05 and (**b**) PD2T cells

biased with an electric voltage, a colorful image behind the PC05 cell was observed. During this period, the PC05 cell exhibited a transparent "on" state, as shown in Fig. 10a. After the electric voltage was removed, the PC05 cell turned from transparent to opaque, and the image disappeared in the "OFF" state, as shown in Fig. 10b. Furthermore, the POM textures of the "ON" and "OFF" states were studied, and the results are shown in Fig. 11. When the PC05 cell was biased with a voltage in the "ON" state, a homeotropic alignment was observed, as indicated by the dark signal in the POM image. During this period, the polarized incident light was not further tuned by the homeotropic LC molecules, forming a dark image, as shown in Fig. 11a. In contrast, in the "OFF" state, as shown in the inset image in Fig. 11b, the polarized incident light is further tuned by focal-conic LC molecules, which exhibit a colorful texture. Video 1 is provided as Supplementary Information showing the real "ON" and "OFF" operations of the fabricated PSCLC cell. The "ON" and "OFF" functions indicate the available electro-optical properties of the fabricated PSCLC cell.

Reliability of fabricated CLC cells

Figure 12 shows the reliability of the fabricated PC05 and PD2T PSCLC cells. The results revealed that the prepared PSCLC cells had stable electro-optical properties. Both the chiral effect and radial constructed particle dopant effect on the LCD were confirmed, clarified and evidenced.

Conclusion

We have developed a straightforward technique for manufacturing LCDs with improved electro-optical features. Radially constructed particles were synthesized and used as dopants for the fabrication of LCD cells. The chiral CNP dopant and the radially constructed PDAT dopant significantly increase the transmittance of the CLC and PSCLC cells, respectively. The fabricated chiral CNP-doped PC05 CLC cell exhibited a high transmittance of 97.4% and a fast response time of 7.6 ms. For the radially constructed PDAT-doped PD2T PSCLC cell, a high transmittance of 93.6% and a fast response time of 13 ms were achieved. The fabrication of LCDs without an alignment layer on substrates was achieved by syndicate adding polymer nanoparticles. Adding 2 wt% chiral CNPs promoted the transmittance of the CLCs from 3.4 to 97%. This novel chiral dopant technique provides a new easy method for the fabrication of LCDs.

Acknowledgements The authors would like to thank the National Science and Technology Council (NSTC) of the Republic of China (Taiwan) for financially supporting this research under Contract MOST 111-2221-E-006-156. This research was also supported in part by the Higher Education Sprout Project, Ministry of Education to the Headquarters of University Advancement at National Cheng Kung University (NCKU).

Compliance with ethical standards

Conflict of interest The authors declare no competing interests.

References

1. Yang B, Wang G, Xia B, Zhong M, Fan P, Chen F, et al. Enzymatic synthesis of chiral polyamide via condensation of natural source amino acid diesters and diamine. Macromol Chem Phys. 2021;222:2100162.
2. Zhang Y, Xia B, Li Y, Lin X, Wu Q. Substrate engineering in lipase-catalyzed selective polymerization of d-/l-aspartates and diols to prepare helical chiral polyester. Biomacromolecules. 2021;22:918–26.
3. Pschyklenk L, Wagner T, Lorenz A, Kaul P. Optical gas sensing with encapsulated chiral-nematic liquid crystals. ACS Appl Polym Mater. 2020;2:1925–32.
4. Yan J, Ota F, San Jose BA, Akagi K. Chiroptical resolution and thermal switching of chirality in conjugated polymer luminescence via selective reflection using a double-layered cell of chiral nematic liquid crystal. Adv Funct Mater. 2017; 27:1604529.
5. Lu X, Zhou Z, Ni B, Li H, Li Y, Li B, et al. Tuning the circularly polarized luminescence of polymer-stabilized cholesteric liquid crystal films using chiral dopants. J Mater Chem C. 2022;10:8246–53.
6. Froyen AAF, Wübbenhorst M, Liu D, Schenning APHJ. Electrothermal color tuning of cholesteric liquid crystals using interdigitated electrode patterns. Adv Electron Mater. 2021;7:2000958.
7. Lu H, Hu J, Chu Y, Xu W, Qiu L, Wang X, et al. Cholesteric liquid crystals with an electrically controllable reflection bandwidth based on ionic polymer networks and chiral ions. J Mater Chem C. 2015;3:5406–11.
8. Lu H, Wang Q, Zhu M, Huang P, Xu M, Qiu L, et al. Electrically controllable reflection bandwidth polymer-stabilized cholesteric liquid crystals with low operating voltage. Liq Cryst. 2022;49:1314–21.
9. Inoue Y, Yoshida H, Inoue K, Shiozaki Y, Kubo H, Fujii A, et al. Tunable lasing from a cholesteric liquid crystal film embedded with a liquid crystal nanopore network. Adv Mater. 2011;23:5498–501.
10. White TJ, McConney ME, Bunning TJ. Dynamic color in stimuli-responsive cholesteric liquid crystals. J Mater Chem. 2010;20:9832–47.
11. Lu P, Chen Y, Chen Z, Yuan Y, Zhang H. Electric field, temperature and light-triggered triple dynamic circularly polarized luminescence switching in fluorescent cholesteric liquid crystals with a large dissymmetry factor. J Mater Chem C. 2021;9:6589–96.
12. Rouhbakhsh Z, Verdian A, Rajabzadeh G. Design of a liquid crystal-based aptasensing platform for ultrasensitive detection of tetracycline. Talanta. 2020;206:120246.
13. Tan H, Yang S, Shen G, Yu R, Wu Z. Signal-enhanced liquid-crystal DNA biosensors based on enzymatic metal deposition. Angew Chem Int Ed. 2010;49:8608–11.
14. Škarabot M, Osmanagič E, Muševič I. Surface anchoring of nematic liquid crystal 8OCB on a DMOAP-silanated glass surface. Liq Cryst. 2006;33:581–5.
15. Zhang Y, Yang W, Gu M, Wei Q, Lv P, Li M, et al. Versatile homeotropic liquid crystal alignment with tunable functionality prepared by one-step method. J Colloid Interface Sci. 2022;608:2290–7.
16. Lee CS, Kumar TA, Kim JH, Lee JH, Gwag JS, Lee G-D, et al. An electrically switchable visible to infra-red dual frequency cholesteric liquid crystal light shutter. J Mater Chem C. 2018;6:4243–9.
17. Kumar P, Kang S-W, Lee SH. Advanced bistable cholesteric light shutter with dual frequency nematic liquid crystal. Opt Mater Express. 2012;2:1121–34.
18. Oh S-W, Baek J-M, Heo J, Yoon T-H. Dye-doped cholesteric liquid crystal light shutter with a polymer-dispersed liquid crystal film. Dyes Pigments. 2016;134:36–40.
19. Oh S-W, Kim S-H, Yoon T-H. Thermal control of transmission property by phase transition in cholesteric liquid crystals. J Mater Chem C. 2018;6:6520–5.
20. Liang X, Chen M, Wang Q, Guo S, Zhang L, Yang H. Active and passive modulation of solar light transmittance in a hybrid thermochromic soft-matter system for energy-saving smart window applications. J Mater Chem C. 2018;6:7054–62.
21. Liu C-Y, Yen C-F, Hung Y-H, Tu C-M, Wu G-Y, Chen H-Y. Polymer-stabilized bistable dual-frequency cholesteric liquid crystal devices assisted by a predesigned chiral dopant. J Mater Chem C. 2021;9:16672–81.
22. Maiti UN, Lee WJ, Lee JM, Oh Y, Kim JY, Kim JE, et al. 25th Anniversary Article: Chemically modified/doped carbon nanotubes & graphene for optimized nanostructures & nanodevices. Adv Mater. 2014;26:40–67.
23. Jian B-R, Tang C-Y, Lee W. Temperature-dependent electrical properties of dilute suspensions of carbon nanotubes in nematic liquid crystals. Carbon. 2011;49:910–4.
24. Ma Z, Han Y, Li Z, Zhang Y, Zhang H, Zheng G, et al. Effects of nematic liquid crystal doped with multi-walled carbon nanotube on electro-optic properties and electrostatic discharge immunity of liquid crystal display device. Liq Cryst. 2023;50:505–18.
25. Cook G, Reshetnyak VY, Ziolo RF, Basun SA, Banerjee PP, Evans DR. Asymmetric Freedericksz transitions from symmetric liquid crystal cells doped with harvested ferroelectric nanoparticles. Opt Express. 2010;18:17339–45.
26. Gdovinová V, Tomašovičová N, Jeng S-C, Zakutanská K, Kula P, Kopčanský P. Memory effect in nematic phase of liquid crystal doped with magnetic and non-magnetic nanoparticles. J Mol Liq. 2019;282:286–91.

27. Gorkunov MV, Osipov MA. Mean-field theory of a nematic liquid crystal doped with anisotropic nanoparticles. Soft Matter. 2011;7:4348–56.
28. Haraguchi F, Inoue K-I, Toshima N, Kobayashi S, Takatoh K. Reduction of the threshold voltages of nematic liquid crystal electrooptical devices by doping inorganic nanoparticles. Jpn J Appl Phys. 2007;46:L796.
29. Kumar A, Prakash J, Khan MT, Dhawan SK, Biradar AM. Memory effect in cadmium telluride quantum dots doped ferroelectric liquid crystals. Appl Phys Lett. 2010;97:163113.
30. Kinkead B, Hegmann T. Effects of size, capping agent, and concentration of CdSe and CdTe quantum dots doped into a nematic liquid crystal on the optical and electro-optic properties of the final colloidal liquid crystal mixture. J Mater Chem. 2010;20:448–58.
31. Lapanik V, Timofeev S, Haase W. Electro-optic properties of nematic and ferroelectric liquid crystalline nanocolloids doped with partially reduced graphene oxide. Phase Transit. 2016;89:133–43.
32. Zhang W, Wang X, Wang D, Yang Z, Gao H, Xing Y, et al. Blue phase liquid crystals affected by graphene oxide modified with aminoazobenzol group. Liq Cryst. 2016;43:573–80.
33. Ni S, Li H, Li S, Zhu J, Tan J, Sun X, et al. Low-voltage blue-phase liquid crystals with polyaniline-functionalized graphene nanosheets. J Mater Chem C. 2014;2:1730–5.
34. Kocakülah G, Algül G, Köysal O. Effect of CdSeS/ZnS quantum dot concentration on the electro-optical and dielectric properties of polymer stabilized liquid crystal. J Mol Liq. 2020;299:112182.
35. Kocakülah G, Balci S, Köysal O. Determination of phase transition and electro-optical behaviors of quantum dot doped polymer dispersed liquid crystal. J Electron Mater. 2020;49:3427–34.
36. Liu X, Wei R, Hoang PT, Wang X, Liu T, Keller P. Reversible and rapid laser actuation of liquid crystalline elastomer micropillars with inclusion of gold nanoparticles. Adv Funct Mater. 2015;25:3022–32.
37. Draper M, Saez IM, Cowling SJ, Gai P, Heinrich B, Donnio B, et al. Self-assembly and shape morphology of liquid crystalline gold metamaterials. Adv Funct Mater. 2011;21:1260–78.
38. Middha M, Kumar R, Raina KK. Effects of chirality on optical and electro-optic behavior of nematic liquid crystals doped with functionalized silver nanoparticles. J Mol Liq. 2016;219:631–6.
39. Singh UB, Dhar R, Dabrowski R, Pandey MB. Influence of low concentration silver nanoparticles on the electrical and electro-optical parameters of nematic liquid crystals. Liq Cryst. 2013;40:774–82.
40. Mishra M, Dabrowski RS, Vij JK, Mishra A, Dhar R. Electrical and electro-optical parameters of 4′-octyl-4-cyanobiphenyl nematic liquid crystal dispersed with gold and silver nanoparticles. Liq Cryst. 2015;42:1580–90.
41. Bednarska K, Oszwa P, Bartosewicz B, Jankiewicz B, Lesiak P, Ertman S, et al. Enhancement of thermal and electro-optical properties of photonic crystal fibers infiltrated with a modified 6CHBT nematic liquid crystal doped with gold nanoparticles. Opt Mater. 2019;98:109419.
42. Wojcik M, Lewandowski W, Matraszek J, Mieczkowski J, Borysiuk J, Pociecha D, et al. Liquid-crystalline phases made of gold nanoparticles. Angew Chem Int Ed. 2009;48:5167–9.
43. Nishida N, Shiraishi Y, Kobayashi S, Toshima N. Fabrication of liquid crystal sol containing capped Ag−Pd bimetallic nanoparticles and their electro-optic properties. J Phys Chem C. 2008;112:20284–90.
44. Kobayashi S, Miyama T, Nishida N, Sakai Y, Shiraki H, Shiraishi Y, et al. Dielectric spectroscopy of metal nanoparticle doped liquid crystal displays exhibiting frequency modulation response. J Disp Technol. 2006;2:121–9.
45. Wu G-Y, Chang K-T, Ou S-Y, Zhuang C-H, Liu C-Y. Polymer beads dispersed liquid crystal devices (PBLCD) achieved by predesigned radially constructed polymeric particles. J Appl Polym Sci. 2022;139:e53037.